Simplified method for the lateral, rotational and torsional static stiffness of circular footings on a non-homogeneous elastic half-space based on a work-equivalent framework

Stephen K. Suryasentana[1], Ph.D.

Paul W. Mayne[2], Ph.D., P.E., M.ASCE

Affiliations

[1] Lecturer, Department of Civil and Environmental Engineering, University of Strathclyde, 75 Montrose St, Glasgow G1 1XJ, UK.

[2] Professor, School of Civil and Environmental Engineering, Georgia Institute of Technology, 790 Atlantic Dr., Mason Building 2245, Atlanta, GA 30332-0355, USA.

Corresponding author information

Stephen K. Suryasentana

stephen.suryasentana@strath.ac.uk

26 April 2021

This is a peer reviewed accepted author manuscript of the following research article:
Suryasentana, S. K., & Mayne, P. W. (2022). Simplified method for the lateral, rotational, and torsional static stiffness of circular footings on a nonhomogeneous elastic half-space based on a work-equivalent framework. Journal of geotechnical and geoenvironmental engineering, 148(2), [2731]. https://doi.org/10.1061/(ASCE)GT.1943-5606.0002731

Abstract

Although there are many methods for assessing the vertical stiffness of footings on the ground, simplified solutions to evaluate the lateral, rotational, and torsional static stiffness are much more limited, particularly for non-homogeneous profiles of shear modulus with depth. This paper addresses the topic by introducing a novel ‘work-equivalent’ framework to develop new simplified design methods for estimating the stiffnesses of footings under multiple degrees-of-freedom loading for general non-homogeneous soils. Furthermore, this framework provides a unified basis to analyze two existing design methods that have diverging results. Three-dimensional finite element analyses were carried out to investigate the soil-footing interaction for a range of continuously varying and multi-layered non-homogeneous soils and to validate the new design approach.

Keywords

Settlement, stiffness, footings, foundations, soil/structure interaction, non-homogeneous modulus, elasticity

NOTATION

z	depth below ground level
D	foundation diameter
$\tilde{z}$	normalized depth with respect to foundation diameter
V	vertical load applied to foundation
H	lateral load applied to foundation
M	rotational moment applied to foundation
Q	torsion applied to foundation
u_z	vertical displacement of foundation
u_H	lateral displacement of foundation
θ_M	rotation of foundation
θ_z	torsional displacement of foundation
G	shear modulus of elastic half-space (soil)
E	Young's modulus of elastic half-space (soil) = $2G(1+\nu)$
ν	Poisson's ratio of elastic half-space (soil)
I_G	displacement influence factor
I_F	foundation rigidity correction factor
q_z	average vertical stress at the soil-foundation interface
$\tilde{\sigma}_z$	normalized vertical stress distribution with respect to q_z
α	factor controlling the rate of increase of the shear modulus with depth
G_{R}	reference shear modulus value
G_{eq}	equivalent constant shear modulus value for a non-homogeneous elastic half-space
U	elastic strain energy of a half-space
u_σ	stress-based energy gradient
w_σ	stress-based weight distribution
u_ε	strain-based energy gradient
w_ε	strain-based weight distribution
K_V	vertical stiffness of the soil-foundation interaction
K_H	lateral stiffness of the soil-foundation interaction
K_M	rotational stiffness of the soil-foundation interaction
K_Q	torsional stiffness of the soil-foundation interaction
p_{atm}	atmospheric pressure

1 Introduction

The assessment of the performance of structures under loading depends on an understanding of the interactions between the soil and the foundation of the structure. For shallow foundations supporting structures such as wind turbines, transmission towers and offshore platforms, special concerns must address the evaluation of soil-foundation response under multiple degrees-of-freedom (DoF) loading, specifically vertical, lateral, rotational and torsional loading. Although there has been much research in assessing soil-foundation response under multiple DoF loading, most of them are focused on the ultimate limit response (e.g. Gourvenec and Randolph 2003; Gourvenec 2007; Nouri et al. 2014; Vulpe et al. 2014; Shen et al. 2017; Dunne and Martin 2017; Suryasentana et al. 2020a, b; He and Newson 2020). The assessment of soil-foundation response at relatively small magnitudes of multiple DoF loading is, however, important for applications such as structural fatigue analysis and natural frequency analysis.

The initial stiffness of the soil-foundation response at relatively small magnitudes of multiple DoF loading can be estimated by assuming that the soil response is approximately linearly elastic at relatively small loads. While there are existing design solutions for representing the initial stiffness under multiple DoF loading, these solutions typically assume a homogeneous elastic soil modulus profile where modulus is constant with depth (e.g. Poulos and Davis 1974; Gazetas 1991), or an idealized non-homogeneous elastic soil modulus profile that conforms to a specific parametric form (e.g. Doherty and Deeks 2003; Doherty et al. 2005; Efthymiou and Gazetas 2018). As soils encountered in real life may deviate from the idealized non-homogeneous profiles, computational methods such as three-dimensional (3D) finite-element methods (FEM) can be used to obtain more realistic estimates of the initial stiffness for the foundation. However, 3D FEM is not always practical for routine design purposes in geotechnical engineering.

Therefore, this paper describes a novel framework for developing new simplified design methods that can provide quick and approximate values of the initial stiffness of rigid circular surface foundations under multiple DoF loading in general non-homogeneous (including multi-

layered) soils. Although this paper restricts its scope to rigid circular surface foundations as an exemplar for the framework, simplified design methods can similarly be developed for other foundation types (different shape, geometry or rigidity), following the procedures described in the paper.

For this paper, V, H, M, Q are defined as the vertical force, lateral force, rotational moment and torsion that is applied to the center of the foundation base, and $u_z, u_H, \theta_M, \theta_z$ are defined as the corresponding vertical displacement, lateral displacement, rotation and torsional displacement of the foundation (see Fig. 1). For homogeneous isotropic linear elastic soil, the reference analytical solutions for the vertical stiffness $K_V = V/u_z$ (Boussinesq 1885), lateral stiffness $K_H = H/u_H$ (Bycroft 1956), rotational stiffness $K_M = M/\theta_M$ (Borowicka 1943), and torsional stiffness $K_Q = Q/\theta_z$ (Reissner and Sagoci 1944) of a rigid circular surface foundation are expressed as follows (Poulos and Davis 1974; API 2002; Kausel 2010):

$$K_V = \frac{2GD}{1-\nu} \tag{1}$$

$$K_H = \frac{16(1-\nu)GD}{7-8\nu} \tag{2}$$

$$K_M = \frac{GD^3}{3(1-\nu)} \tag{3}$$

$$K_Q = \frac{2GD^3}{3} \tag{4}$$

where D is the foundation diameter, G is the (assumed homogeneous) shear modulus of the soil, and ν is the soil Poisson's ratio. Many natural soil formations exhibit a non-homogeneous shear modulus profile, however, where the stiffness is represented by a continuously varying shear modulus with depth; specifically, the initial shear modulus G_0 increases with mean effective stress p' in accordance with a power law format:

$$G_0 = G_R \left(\frac{p'}{p_{\text{atm}}} \right)^n \tag{5}$$

where p_{atm} is the atmospheric pressure, G_R is the reference shear modulus at atmospheric pressure, and n varies from approximately 0.5 for sands (Hardin and Black 1966, Wroth et al. 1979, Kohata et al. 1997, Houlsby et al. 2005) to 1.0 for clays (Hardin and Black 1968, Shibuya et al. 1997; Yamada et al. 2008).

For non-homogeneous linear elastic soil, there is considerable work regarding vertical stiffness in non-homogeneous ground (e.g. Gibson 1967; Carrier and Christian 1973; Kassir and Chuaprasert 1974; Boswell and Scott 1975; Vrettos 1991; Selvadurai 1996; Doherty and Deeks 2003). One such design method is that proposed by Mayne and Poulos (1999), for which the general form is:

$$u_z = q_z D I_F \int_0^h \frac{\tilde{\sigma}_z - 2\nu\tilde{\sigma}_r}{E}\, d\tilde{z} \tag{6}$$

where

$$\tilde{\sigma}_z = \frac{\sigma_z}{q_z} = 1 - \frac{1}{(1 + (0.5/\tilde{z})^2)^{1.5}} \tag{7}$$

$$\tilde{\sigma}_r = \frac{\sigma_r}{q_z} = \frac{1}{2} + \nu - \frac{1+\nu}{((0.5/\tilde{z})^2 + 1)^{0.5}} + \frac{0.5}{((0.5/\tilde{z})^2 + 1)^{1.5}} \tag{8}$$

$$\tilde{z} = \frac{z}{D} \tag{9}$$

in which E is the Young's modulus of the soil (which may vary with depth), z is the depth below ground level, $\tilde{z}$ is the normalized depth with respect to the foundation diameter D, σ_z is the Boussinesq vertical stress distribution (Boussinesq 1885), σ_r is the horizontal stress distribution for axisymmetric uniform loading (Poulos and Davis 1974) and q_z is the average vertical stress applied at the soil-foundation interface. I_F is the rigidity correction factor and equals $\frac{\pi}{4}$ for perfectly rigid foundations and 1 for perfectly flexible foundations. For the special case of linearly increasing Young's Modulus for the soil, Eq. 6 simplifies to:

$$u_z = \frac{q_z D I_F I_G (1 - \nu^2)}{E_0} \tag{10}$$

where E_0 is the value of the soil Young's Modulus directly beneath the foundation base ($z = 0$) and I_G is the displacement influence factor whose values can be obtained from the design charts in Mayne and Poulos (1999), or in closed-form in Mayne (2019).

Another widely cited design method for estimating the vertical stiffness comes from the field of contact mechanics, where Gao et al. (1992) proposed the following to represent the settlement of a rigid cylindrical punch on a non-homogeneous elastic half-space:

$$u_z = \frac{V}{2D}\left(\frac{1-\int_0^\infty \frac{dI_1}{dz}\nu\, dz}{\int_0^\infty \frac{dI_0}{dz}G\, dz}\right) \tag{11}$$

where

$$I_0 = \frac{2}{\pi}\arctan(2\tilde{z}) + \frac{(1-2\nu)(2\tilde{z})\ln\left(\frac{1+(2\tilde{z})^2}{(2\tilde{z})^2}\right) - \frac{(2\tilde{z})}{1+(2\tilde{z})^2}}{2\pi(1-\nu)} \tag{12}$$

$$I_1 = \frac{2}{\pi}\arctan(2\tilde{z}) + \frac{2\tilde{z}}{\pi}\ln\left(\frac{1+(2\tilde{z})^2}{(2\tilde{z})^2}\right) \tag{13}$$

Eq. 11 is a closed-form solution that was derived using a first-order rigorous moduli-perturbation method, where the reference solution for a homogeneous elastic half-space is used to estimate the change in settlement in non-homogeneous elastic half-spaces.

For the evaluation of the lateral, rotational, and torsional stiffness of surface foundations on non-homogeneous elastic soil, most previous research efforts use computational procedures such as the scaled boundary FEM (e.g. Doherty et al. 2005; Birk and Behnke 2012) to obtain estimates of these stiffnesses. Semi-analytical approaches based on the Green's function (e.g. Andersen and Clausen 2008; Lin et al. 2013) and simplified approaches (Anam and Roësset 2004) have been proposed to estimate the dynamic stiffness of surface foundations on multi-layered elastic soils. However, there is a lack of simplified design methods that is amenable to simple spreadsheet calculations, which can estimate the lateral, rotational and torsional static stiffness of circular surface foundations on soil with general non-homogeneous (including multi-layered) shear modulus profiles, similar to Eqs. 6 and 11 for the vertical stiffness problem.

Therefore, this paper aims to address this limitation by introducing a novel 'work-equivalent' framework that reveals a property of the elastic half-space that stays approximately invariant to changes to the shear modulus. This framework is then used to develop new simplified design methods to estimate the stiffness of the foundation on non-homogeneous elastic soil under multiple DoF loading. This is a timely contribution as there is little guidance in the design codes (e.g. API 2002) for this common design problem. Furthermore, this paper demonstrates that the proposed framework provides a common basis to compare Eqs. 6 and 11 and helps shed light

on the possible causes for their diverging performance. Moreover, it bears the advantage of allowing one single implementation to reproduce both design methods.

2 Work-equivalent framework

The work-equivalent framework is a framework that allows any non-homogeneous linear elastic half-space to be transformed into a work-equivalent homogeneous elastic half-space. In other words, a non-homogeneous half-space with some arbitrary shear modulus profile can be converted into a homogeneous half-space with a constant shear modulus, which is defined such that both half-spaces are 'work-equivalent'. Under this framework, two linear elastic half-spaces are 'work-equivalent' if it takes the same amount of work to produce the same amount of displacement on both half-spaces. Conservation of energy then implies that two 'work-equivalent' linear elastic half-spaces have the same amount of elastic strain energy.

To better illustrate the framework, consider the transformation of a non-homogeneous elastic half-space H_1 into its work-equivalent, homogeneous counterpart H_{eq}. The value of H_{eq} may be determined using two methods, depending on the key assumptions adopted. The following exposition will describe the first method and its associated assumptions, before describing the second method.

First method

Consider the elastic strain energy U of a half-space:

$$U = \iiint \sum_{i,j} \frac{1}{2} \sigma_{\mathrm{ij}} \varepsilon_{\mathrm{ij}} \, dxdydz \tag{14}$$

where σ_{ij}, $\varepsilon_{\mathrm{ij}}$ are the stress and strain components of the half-space and the integration is carried out over the entire volume of the half-space. From linear elasticity theory, it is known that:

$$\varepsilon_{\mathrm{ij}} = \frac{(1+\nu)\sigma_{\mathrm{ij}} - \nu\delta_{\mathrm{ij}} \sum_k \sigma_{\mathrm{kk}}}{2(1+\nu)G} \tag{15}$$

where δ_{ij} is the Kronecker delta.

Substituting Eq. 15 into Eq. 14 gives:

$$U = \iiint \sum_{i,j} \frac{1}{2}\sigma_{ij}\left(\frac{(1+\nu)\sigma_{ij} - \nu\delta_{ij}\sum_k \sigma_{kk}}{2(1+\nu)G}\right) dxdydz \tag{16}$$

As this paper is only concerned with non-homogeneous shear modulus profiles that vary with depth (i.e. $G = G(z)$), Eq. 16 simplifies to:

$$U = \int_0^\infty \frac{1}{G} u_\sigma dz \tag{17}$$

where

$$u_\sigma = \iint \sum_{i,j} \frac{1}{2}\sigma_{ij}\left(\frac{(1+\nu)\sigma_{ij} - \nu\delta_{ij}\sum_k \sigma_{kk}}{2(1+\nu)}\right) dxdy \tag{18}$$

As u_σ is calculated using the stress components and Eq. 17 implies that $u_\sigma = \frac{\partial U}{\partial z} G$, the parameter u_σ shall be termed the 'stress-based energy gradient'.

Now, let U_1 and U_{eq} be the elastic strain energy of H_1 and H_{eq} respectively:

$$U_1 = \int_0^\infty \frac{1}{G}(u_\sigma)_1 \, dz \tag{19}$$

$$\mathrm{U_{eq}} = \frac{1}{G_{\mathrm{eq}}}\int_0^\infty (u_\sigma)_{\mathrm{eq}} \, dz \tag{20}$$

where G_{eq} is the 'equivalent shear modulus' for H_{eq}.

Since H_1 and H_{eq} are work-equivalent, $U_1 = U_{\mathrm{eq}}$:

$$\frac{1}{G_{\mathrm{eq}}}\int_0^\infty (u_\sigma)_{\mathrm{eq}} \, dz = \int_0^\infty \frac{1}{G}(u_\sigma)_1 \, dz \tag{21}$$

$$\frac{1}{G_{\mathrm{eq}}} = \int_0^\infty \frac{1}{G} w_\sigma \, dz$$

where

$$w_\sigma = \frac{(u_\sigma)_1}{\int_0^\infty (u_\sigma)_{\mathrm{eq}} \, dz} \tag{22}$$

Suppose the following assumption is true.

Assumption 1: w_σ is approximately invariant to changes in the shear modulus profile.

If Assumption 1 is true, there exists a unique weight distribution w_σ (for a fixed ν) that can be used to compute G_{eq} for any non-homogeneous half-space using Eq. 21. Since w_σ is calculated using the stress-based energy gradient u_σ, w_σ shall be termed the 'stress-based weight distribution'.

Second method

It is also known from linear elasticity theory that:

$$\sigma_{\mathrm{ij}} = 2G\left(\frac{\nu}{1-2\nu}\delta_{\mathrm{ij}}\sum_{k}\varepsilon_{kk} + \varepsilon_{\mathrm{ij}}\right) \tag{23}$$

Substituting Eq. 23 into Eq. 14 and following the same procedure as before produces:

$$U = \int_0^\infty G u_\varepsilon \, dz \tag{24}$$

where

$$u_\varepsilon = \iint \sum_{i,j}\frac{1}{2}\varepsilon_{\mathrm{ij}}\left(\frac{2\nu}{1-2\nu}\delta_{\mathrm{ij}}\sum_{k}\varepsilon_{\mathrm{kk}} + 2\varepsilon_{\mathrm{ij}}\right)dxdy \tag{25}$$

As u_ε is calculated using the strain components and Eq. 24 implies that $u_\varepsilon = \frac{\partial U}{\partial z}\frac{1}{G}$, the parameter u_ε shall be termed the 'strain-based energy gradient'.

Since H_1 and H_{eq} are work-equivalent, their elastic strain energy can be equated to give:

$$G_{\mathrm{eq}}\int_0^\infty (u_\varepsilon)_{\mathrm{eq}}\, dz = \int_0^\infty G(u_\varepsilon)_1\, dz \tag{26}$$

$$G_{\mathrm{eq}} = \int_0^\infty G\, w_\varepsilon\, dz$$

where

$$w_\varepsilon = \frac{(u_\varepsilon)_1}{\int_o^\infty (u_\varepsilon)_{\mathrm{eq}}\, dz} \tag{27}$$

Suppose the following assumption is true.

Assumption 2: w_ε is approximately invariant to changes in the shear modulus profile.

If Assumption 2 is true, there exists a unique weight distribution w_ε (for a fixed Poisson's ratio ν) that can be used to compute G_{eq} for any non-homogeneous half-space using Eq. 26. Since w_ε is calculated using the strain-based energy gradient u_ε, w_ε is termed the 'strain-based weight distribution'.

2.1 Weighted average shear modulus

The work-equivalent framework suggests that if one of the above assumptions is true, there exists some invariant weight distribution that can convert any non-homogeneous half-spaces into work-equivalent homogeneous half-spaces using either Eq. 21 or Eq. 26. This would involve finding the weighted average of the shear modulus after treating the *x-y* planes of the half-space as 'springs in series' (if w_σ invariance is assumed) or 'springs in parallel' (if w_ε invariance is assumed).

3 Assessment of assumptions

To assess the validity of the two assumptions, a 3D FEM study was carried out using the commercial FEM software Abaqus v6.13 (Dassault Systèmes 2014). The 3D FEM model consists of a rigid circular surface foundation of diameter D on non-homogeneous elastic soil with continuously varying shear modulus profiles (see Fig. 1) of the following form:

$$G = G_R\left(\frac{2z}{D}\right)^{\alpha} \tag{28}$$

where D is the diameter of the foundation, α is a factor controlling the rate of increase of the shear modulus with depth ($\alpha = 0$ represents homogeneous G) and G_R is a reference shear modulus. Eq. 28 has the same parametric form as that adopted by Doherty et al. (2005).

The soil volume is defined as weightless and isotropic linear elastic. Four continuously varying shear modulus profiles ($\alpha = 0, 0.2, 0.6,$ and 1 in Eq. 28), and six values of Poisson's ratio ($\nu = 0, 0.1, 0.2, 0.3, 0.4, 0.49$) are analysed. Note that although six Poisson's ratio values are analysed, the figures in this paper only show the results for the practical values of $\nu = 0.2, 0.49$

(corresponding to drained sandy and undrained clayey materials, respectively) for illustrative purposes. First-order, fully integrated, linear, brick elements C3D8 (or C3D8H for $\nu = 0.49$) are assigned to the soil elements. These elements are adequate as comparisons with initial analyses using their higher-order counterparts (C3D20 or C3D20H) showed insignificant differences.

The mesh domain is set to $100D$ for both width and depth, which is large enough to avoid boundary effects based on preliminary results. Mesh convergence analyses have been carried out to determine the mesh fineness. The 3D FEM mesh is shown in Fig. 2. Displacements are fixed in all directions at the bottom of the mesh domain and in the radial directions on its periphery. The surface foundation was modelled as a weightless, rigid body, and the loading reference point RP was set at the center of its base, as shown in Fig. 1. Separation and slip at the soil-foundation interface was prevented using tie constraints. Vertical, lateral, rotational and torsional displacements are independently prescribed at the reference point RP to obtain the vertical, lateral, rotational and torsional stiffness, respectively.

3.1 Assessment of Assumptions 1 and 2

To assess Assumptions 1 and 2, a pair of 3D FEM analysis is investigated for every non-homogeneous shear modulus profile. Each pair consists of a 3D FEM analysis of the footing on a non-homogeneous shear modulus profile and another 3D FEM analysis that is identical to the former, except that the shear modulus profile is now constant with depth and the constant shear modulus value is set such that both analyses result in the same work done by the footing. These pair of 3D FEM analyses can then be used to calculate w_σ and w_ε, following the steps described in Appendix A.

Figs. 3 and 4 compare the calculated values of w_σ and w_ε for the different non-homogeneous shear modulus profiles. It is evident that w_σ stays approximately the same, while w_ε changes significantly, for all displacement types. Therefore, the results provide strong support for Assumption 1, but not for Assumption 2.

4 Existing design methods for vertical stiffness

One benefit of the work-equivalent framework is that it provides a common basis to compare existing (and seemingly disparate) design methods for estimating the vertical stiffness. First, Eqs. 6 and 11 are reproduced exactly using the work-equivalent framework. For example, Eq. 6 can be reproduced as (see Appendix B):

$$K_V = \frac{2D}{1-\nu} G_{\mathrm{MP}} \tag{29}$$

where

$$G_{\mathrm{MP}} = \frac{1-\nu^2}{\int_0^\infty \frac{1}{G}(\tilde{\sigma}_z - 2\nu\tilde{\sigma}_r) d\tilde{z}} \tag{30}$$

G_{MP} can be manipulated into the form of Eq. 21 as follows:

$$\frac{1}{G_{\mathrm{MP}}} = \int_0^\infty \frac{1}{G} w_{\mathrm{MP}}\, d\tilde{z} \tag{31}$$

where

$$w_{\mathrm{MP}} = \frac{\tilde{\sigma}_z - 2\nu\tilde{\sigma}_r}{1-\nu^2} \tag{32}$$

Similarly, Eq. 11 (for a fixed Poisson's ratio, ν) can be reproduced as (see Appendix C):

$$K_V = \frac{2D}{1-\nu} G_{\mathrm{GCL}} \tag{33}$$

where

$$G_{\mathrm{GCL}} = \int_0^\infty G\, w_{\mathrm{GCL}}\, d\tilde{z} \tag{34}$$

$$w_{\mathrm{GCL}} = \frac{dI_0}{d\tilde{z}} \tag{35}$$

It can be observed that Eqs. 29 and 33 have the same form as the reference vertical stiffness solution for a homogeneous elastic half-space (i.e. Eq. 1), where the constant shear modulus in Eq. 1 is now replaced by an equivalent, weighted shear modulus (i.e. G_{MP} or G_{GCL}). Thus, this suggests that Eqs. 6 and 11 can be viewed as belonging to the same class of weighted shear modulus design methods, albeit with different ways of applying the weights.

The same 3D FEM model described in Section 3 was used to carry out additional FEM analyses for the vertical stiffness problem, with the only difference being the application of a smooth constraint at the soil-foundation interface (i.e. soil is free to move horizontally at the interface) in order to match the assumptions behind Eqs. 6 and 11. Fig. 5 compares the vertical stiffness estimations of Eqs. 29 and 33 with these 3D FEM results. Note that the numerical integration of Eq. 31 starts from a small depth (z/D = 10^{-5}) to avoid a singularity when the shear modulus is zero at the ground level. It is evident from Fig. 5 that the Mayne and Poulos (1999) estimations agree well with the 3D FEM results, while the Gao et al. (1992) estimations agree only at low levels of non-homogeneity (i.e. low α values).

To better understand the possible reasons behind the diverging performance of these two design methods, Fig. 6 compares the weight distributions w_σ and w_ε calculated from the 3D FEM results, which shows stronger support for Assumption 1 than for Assumption 2. w_{MP} and w_{GCL} are also shown in Fig. 6 for comparison, which shows that w_{MP} agrees well with the calculated weight distributions w_σ. Fig. 6(c), (d) also explains why Eq. 33 estimates increasing stiffness with increasing α in Fig. 5, as there is a larger weighting of the higher shear modulus at greater depths compared to the true weight distribution, which results in an overestimated equivalent shear modulus. It can also be observed that the type of constraint at the interface has little influence on the assumptions assessments, as there is negligible difference between Fig. 6 and its corresponding results when a fully tied constraint is applied at the interface i.e. compare Fig. 6(a), (b) with Fig. 3(a), (b), and Fig. 6(c), (d) with Fig. 4(a), (b). In summary, Fig. 6 shows stronger support for the underlying assumptions behind Eq. 29 (i.e. Assumption 1) than those behind Eq. 33 (i.e. Assumption 2), which possibly explains the diverging performance of these two design methods.

5 New design methods for lateral, rotational and torsional stiffness

In general, Fig. 3 indicates support for Assumption 1 for all displacement types. Thus, Assumption 1 is adopted to develop the following new design methods to estimate the lateral, rotational and torsional stiffness of rigid circular surface foundations on non-homogeneous soils:

$$K_H = \frac{16(1-\nu)D}{7-8\nu} G_{\mathrm{eq}} \tag{36}$$

$$K_M = \frac{D^3}{3(1-\nu)} G_{\mathrm{eq}} \tag{37}$$

$$K_Q = \frac{2D^3}{3} G_{\mathrm{eq}} \tag{38}$$

where G_{eq} is the constant, equivalent shear modulus that is calculated using Eq. 21 (note that w_σ is different for each stiffness in Eq. 21).

To determine the weight distribution w_σ for each stiffness, new parametric equations $\widehat{w}_{\mathrm{param}}$ are derived to approximate the invariant weight distributions shown in Fig. 3. For simplicity, these parametric equations are assumed to have the form of the Weibull distribution,

$$\widehat{w}_{\mathrm{param}} = \frac{a}{b}\left(\frac{\tilde{z}}{b}\right)^{a-1} \exp\left[-\left(\frac{\tilde{z}}{b}\right)^{a}\right] \qquad \text{for } \tilde{z} \geq 0 \tag{39}$$

where a, b are the Weibull parameters.

Least squares regression is carried out to identify the optimal Weibull parameter values that best fit the true weight distributions calculated from the 3D FEM results for each Poisson's ratio ν, under the constraint that $a > 1$. This constraint is applied so that there is zero weight at the ground level (i.e. $\widehat{w}_{\mathrm{param}} = 0$ at $\tilde{z} = 0$), in order to accommodate zero shear modulus at the ground level in Eq. 21. Consequently, there is some loss of accuracy in the match between the best-fit $\widehat{w}_{\mathrm{param}}$ and the weight distributions calculated from the 3D FEM results; however, this is considered as an acceptable trade-off for the convenience of being able to accommodate zero shear modulus at the ground level (as is commonly idealised for real world soil profiles).

After obtaining the best-fit Weibull parameters for each Poisson's ratio ν, the Weibull parameter a was found to vary insignificantly with ν. Least squares regression is then carried out to fit a power law-based equation ($b = b_0 + b_1\nu^{b_2}$) for the Weibull parameter b in terms of ν. The resultant equations for the Weibull parameters are listed in Table 1. Fig. 7 shows the fit between these equations and the best-fit Weibull parameters for each Poisson's ratio ν. Fig. 3 also shows the resultant Weibull-based parametric weight distributions $\widehat{w}_{\mathrm{param}}$ for estimating the lateral, rotational and torsional stiffness of the foundation, where it is evident that the parametric weight distributions capture the salient trends of the true weight distributions calculated from the 3D FEM analyses.

In summary, there are three design methods (Eqs. 36 to 38) for estimating K_H, K_M, and K_Q, respectively. Each of these design methods has a different Weibull-based weight distribution $\widehat{w}_{\mathrm{param}}$ to evaluate G_{eq}. The weight distribution $\widehat{w}_{\mathrm{param}}$ can be derived by using the relevant equations for the Weibull parameters (a, b), as shown in Table 1. G_{eq} can then be calculated using Eq. 21. For practical purposes, it is sufficient to integrate Eq. 21 to a depth of $20D$, instead of infinite depth, as $\int_0^{20} \widehat{w}_{\mathrm{param}}\, d\tilde{z} \approx 1$. However, if there is a rock bed at, or if there is limited ground data up to, a shallower depth of $z/D = h$, Eq. 21 should be integrated to this depth and G_{eq} should be calculated using the following normalized parametric weight distribution:

$$\widehat{w}_{\mathrm{param}}^{\mathrm{norm}} = \frac{\widehat{w}_{\mathrm{param}}}{\int_0^{\mathrm{h}} \widehat{w}_{\mathrm{param}}\, d\tilde{z}} \tag{40}$$

This will ensure that the $\widehat{w}_{\mathrm{param}}^{\mathrm{norm}}$ is a normalized weight distribution that sums up to 1 (as is the case for the Weibull distribution). A summary of the workflow for estimating the stiffness using the new design methods is shown in Fig. 8.

To validate the new design methods, the stiffness values calculated using Eqs. 36 to 38 are compared with those calculated using the 3D FEM analyses, as shown in Fig. 9. It can be observed that the estimations of the proposed design methods agree well with the 3D FEM results, with the maximum deviations being 6.48%, 9.54% and 3.70% for K_H, K_M and K_Q, respectively.

6 Assessment of proposed design methods in complex soil profiles

Although the proposed design methods may be readily applied to any arbitrary non-homogeneous soils, their reliability for complex (e.g. multi-layered) grounds with shear modulus profiles that deviate from the idealized form (Eq. 28) have not been validated. Therefore, to validate this, 11 complex soil profiles were investigated.

The first two soil profiles correspond to multi-layered clay soil profiles that are representative of realistic ground conditions for offshore wind farm sites (Burd et al. 2020). The first soil profile (termed ‘BC clay’ profile) has soft clay (Bothkennar clay) overlying stiff overconsolidated clay till (Cowden till). The second soil profile (termed ‘BCB clay’ profile) is a Bothkennar clay soil matrix with an interbedded Cowden till layer (see Fig. 10 for the schematic diagrams). These soil profiles were first investigated to validate the application of a pile design model for layered soil conditions. The third soil profile (termed ‘EURIPIDES’ profile) corresponds to a sand test site for the EURIPIDES project (Niazi and Mayne 2010), which investigated the performance of axially-loaded piles in dense sand. The shear moduli of these three soil profiles are shown in Fig. 11. The remaining eight soil profiles correspond to three-layered soil profiles similar to those investigated by Poulos (1979) for his comparisons of solutions for settlement of piles in layered soil. The Young’s modulus of each soil layer is assumed to be constant and Table 2 lists the values of the Young’s modulus and Poisson’s ratio for each soil profile (referred to as P1 to P8 in this paper).

Collectively, these 11 soil profiles are highly challenging for existing design methods (e.g. Doherty et al. 2005), as these design methods typically require an idealized shear modulus form and it is not straightforward to enforce a ‘best-fit’ of the idealized form (Eq. 28) to these complex soil profiles. In contrast, these soil profiles do not pose difficulties for the proposed design methods, since no fitting to an idealized form is required.

To validate the proposed design methods, 3D FEM calculations are carried out to estimate the soil-foundation stiffness using the same FEM model described in Section 3, except for the different shear modulus profiles. A foundation diameter D of 10m is adopted for this numerical study. Sand and clay soils are assigned a Poisson's ratio of 0.2 and 0.49, respectively.

The proposed design methods are used to estimate the lateral, rotational and torsional stiffness of the foundation in these soil profiles. Fig. 12 compares these estimated stiffness values with their corresponding 3D FEM calculated values, which shows that the proposed method performs reasonably well in these challenging ground conditions. For the soil profiles that are more representative of real world ground conditions (i.e. BC clay, BCB clay and EURIPIDES), the estimated values for K_H and K_Q agree very well with the 3D FEM values, with the average deviations being 1.02% and 2.71% for K_H and K_Q, respectively, and the maximum deviations being 1.44% and 3.88% for K_H and K_Q, respectively. The K_M estimations also agree reasonably well with the 3D FEM calculated values, with the average deviation being 8.62% and the maximum deviation being 12.23%, which is broadly in line with the maximum deviation of 9.54% obtained for the calibration cases in Fig. 9 (b). For the P1 to P8 soil profiles, the estimated values for K_Q agree very well with the 3D FEM values, with the average deviation being 3.3% and the maximum deviation being 5.17%. The estimated values for K_H and K_M agree reasonably well with the 3D FEM values, with the average deviations being 10.93% and 9.27% for K_H and K_M, respectively, and the maximum deviations being 17.76% and 17.83% for K_H and K_M, respectively.

Compared to existing simplified design methods, the proposed design methods are more versatile as they can be applied to both continuously varying and multi-layered soil profiles (although it is noted that their accuracies have only been validated for a finite number of soil profiles due to practical reasons). Compared to 3D FEM analyses, the proposed design methods are much faster and more computationally efficient. For example, each 3D FEM analysis in this study took an average of 5 minutes (not including the non-negligible model setup time) to estimate the static stiffness, while the proposed design methods took less than a second. This is particularly important for running sensitivity analysis or for the design of large-

scale projects such as wind farms, where there is need for a large number of rapid and low-cost calculations for the optimal sizing of many foundations in variable ground conditions. Nevertheless, different analysis models are well-suited to meet the requirements at different design stages. At the preliminary design stage, a simplified model such as those recently published (e.g. Bordón et al. 2021) or those proposed in this paper would be sufficient to estimate the foundation stiffness at very low cost; while rigorous but more computationally intensive models such as 3D FEM would be more appropriate for verification of design at the final design stages and for modelling very complex, rarely encountered soil profiles or unconventional distributions of soil-foundation interface pressure.

7 Conclusions

Simplified design methods were derived for evaluating the lateral, rotational and torsional static stiffness of circular surface foundations on general non-homogeneous (including multi-layered) elastic soil; they can be implemented numerically using a simple spreadsheet approach. These design methods were obtained using a novel approach called the ‘work-equivalent’ framework, which shows that there exists some invariant weight distribution that can be used to convert any non-homogeneous half-spaces into ‘work-equivalent’ homogeneous half-spaces. 3D FEM analyses were carried out to validate the assumptions behind this framework and to determine the weight distributions for each stiffness. Moreover, this framework is used as a common basis to analyse two existing design methods for estimating the vertical stiffness of the foundation, which elucidates the plausible reason behind the diverging results of the two design methods.

The proposed design methods have been verified for selected continuously varying shear modulus profiles that cover the range of practical interest for homogeneous clayey or sandy grounds. 11 complex, multi-layered shear modulus profiles were also assessed to validate the proposed design methods in more challenging ground conditions, which showed good results by the proposed design methods. Further studies are desirable to verify the robustness of the proposed design methods for a much larger dataset of real world soil profiles.

8 Data Availability

Some or all data, models, or code that support the findings of this study are available from the corresponding author upon reasonable request.

9 Acknowledgements

Parts of the work described here were conducted during the DPhil studies of the first author at the University of Oxford. The first author would like to thank Professor Byron Byrne, Professor Harvey Burd and Mr Avi Shonberg for their generous support during the studies, and Ørsted Wind Power for funding the DPhil studentship.

10 Appendix

A: Calculation of w_σ and w_ε from 3D FEM results

u_σ and u_ε can be calculated using the following alternative forms of Eqs. 17 and 26:

$$u_\sigma = \frac{\partial U}{\partial z} G \tag{A1}$$

$$u_\varepsilon = \frac{\partial U}{\partial z} \frac{1}{G} \tag{A2}$$

where $\frac{\partial U}{\partial z}$ can be approximated from the 3D FEM results through numerical differentiation of the U distribution, noting that ΔU at each depth can be calculated by summing up the elastic strain energy of all soil elements at that depth (all soil elements at each depth have the same height as a structured mesh is used).

For each 3D FEM analysis for a non-homogeneous shear modulus profile, there is a corresponding 3D FEM analysis that is identical to the former, except that its shear modulus is now constant with depth and its shear modulus value is set such that both analyses result in the same work done by the footing. The former analysis provides the values of $(u_\sigma)_1$ and $(u_\varepsilon)_1$ in Eqs. 22 and 27, while the latter analysis (with the constant shear modulus profiles) provides the values of $\int_o^\infty (u_\sigma)_{\mathrm{eq}}\, dz$ and $\int_o^\infty (u_\varepsilon)_{\mathrm{eq}}\, dz$ in Eqs. 22 and 27.

B: Derivation of design method equivalent to Mayne and Poulos (1999)

The main principle behind the design method of Mayne and Poulos (1999) is that the vertical displacement u_z at the center of the foundation base is the integration of the vertical strains directly beneath it:

$$u_z = \int_0^\infty \varepsilon_z \, dz \tag{B1}$$

$$u_z = D \int_0^\infty \frac{\sigma_z - 2\nu\sigma_r}{E} \, d\tilde{z}$$

$$u_z = \frac{q_z D}{2(1+\nu)} \int_0^\infty \frac{\tilde{\sigma}_z - 2\nu\tilde{\sigma}_r}{G} \, d\tilde{z}$$

$$u_z\left(\frac{\pi D^2}{4}\right) = \frac{VD}{2(1+\nu)} \int_0^\infty \frac{\tilde{\sigma}_z - 2\nu\tilde{\sigma}_r}{G} \, d\tilde{z}$$

$$\frac{V}{u_z} = \left(\frac{\pi D(1+\nu)}{2(1-\nu^2)}\right) \frac{(1-\nu^2)}{\int_0^\infty \frac{\tilde{\sigma}_z - 2\nu\tilde{\sigma}_r}{G} \, d\tilde{z}}$$

$$K_{\mathrm{V}} = \left(\frac{\pi D}{2(1-\nu)}\right) G_{\mathrm{MP}}$$

Eq. B1 estimates the stiffness of a flexible, circular surface foundation. For a rigid, circular surface foundation, a factor of $\frac{\pi}{4}$ (Mayne and Poulos 1999) should be applied such that $(u_z)_{\mathrm{rigid}} = \left(\frac{\pi}{4}\right)(u_z)_{\mathrm{flexible}}$, which produces Eq. 29.

C: Derivation of design method equivalent to Gao et al. (1992)

Assuming that the Poisson's ratio ν is constant with depth, the following shows how Eq. 33 can be derived from Eq. 11, which was proposed by Gao et al. (1992):

$$u_z = \frac{V}{2D}\left(\frac{1-\int_0^\infty \frac{dI_1}{dz}\nu\, dz}{\int_0^\infty \frac{dI_0}{dz} G\, dz}\right) \tag{C1}$$

$$\frac{V}{u_z} = 2D\left(\frac{\int_0^\infty \frac{dI_0}{dz} G\, dz}{1-\int_0^\infty \frac{dI_1}{dz}\nu\, dz}\right)$$

$$K_V = \frac{2D}{1-\nu}\left(\int_0^\infty \frac{dI_0}{dz} G\, dz\right)$$

$$K_V = \frac{2D}{1-\nu}\left(\int_0^\infty \frac{dI_0}{d\tilde{z}} G\, d\tilde{z}\right)$$

$$K_V = \frac{2D}{1-\nu}\left(\int_0^\infty w_{\mathrm{GCL}}\, G\, d\tilde{z}\right)$$

References

Anam, I., and Roësset, J. M. (2004). Dynamic stiffnesses of surface foundations: an explicit solution. International Journal of Geomechanics, 4(3), 216-223.

Andersen, L., and Clausen, J. (2008). Impedance of surface footings on layered ground. Computers and Structures, 86(1-2), 72-87.

API (2002), Recommended Practice for Planning, Designing and Constructing Fixed Offshore Platforms — Working Stress Design, 21st edition, American Petroleum Institute, Washington, D.C.

Birk, C., and Behnke, R. (2012). A modified scaled boundary finite element method for three-dimensional dynamic soil-structure interaction in layered soil. International Journal for Numerical Methods in Engineering, 89(3), 371-402.

Bordón, J. D. R., Aznárez, J. J., Maeso, O., and Bhattacharya, S. (2021). Simple approach for including foundation–soil–foundation interaction in the static stiffnesses of multi-element shallow foundations. Géotechnique, 1-14. https://doi.org/10.1680/jgeot.19.P.005

Borowicka, H. (1943), 'Uber ausmittig belastete, starre Platten auf elastich-isotropem Untergrund', Archive of Applied Mechanics 14, 1–8.

Boswell, L. F. and Scott, C. R. (1975), A flexible circular plate on a heterogeneous elastic halfspace: influence coefficients for contact stress and settlement, Géotechnique 25(3), 604–610.

Boussinesq, M. J. (1885), Application des potentiels a l'etude de l'equilibre et du movement des solides elastiques, principalement au calcul des deformations et des pressions que produisent, dans ces solides, des efforts quelconques exerces sur une petite partie de leur surface , Technical report, GauthierVillars, Paris.

Burd, H. J., Abadie, C. N., Byrne, B. W., Houlsby, G. T., Martin, C. M., McAdam, R. A., Jardine, R.J., Pedro, A.M., Potts, D.M., Taborda, D.M., Zdravković, L., and Andrade, M.P. (2020). Application of the PISA Design Model to Monopiles Embedded in Layered Soils. Géotechnique 70(11): 1-55. https://doi.org/10.1680/jgeot.20.PISA.009

Bycroft, G. (1956). Forced vibrations of a rigid circular plate on a semi-infinite elastic space and on an elastic stratum. Philosophical Transactions of the Royal Society of London. Series A, Mathematical and Physical Sciences, 248(948), 327-368.

Carrier, W. D. and Christian, J. T. (1973), Rigid circular plate resting on a non-homogeneous elastic half-space, Géotechnique 23(1), 67–84.

Doherty, J. P., and Deeks, A. J. (2003). Scaled boundary finite-element analysis of a non-homogeneous elastic half-space. International Journal for Numerical Methods in Engineering, 57(7), 955-973.

Doherty, J. P., Houlsby, G. T. and Deeks, A. J. (2005), Stiffness of flexible caisson foundations embedded in nonhomogeneous elastic soil, Journal of Geotechnical and Geoenvironmental Engineering 131 (12), 1498–1508.

Dunne, H. P., and Martin, C. M. (2017). Capacity of rectangular mudmat foundations on clay under combined loading. Géotechnique, 67(2), 168-180.

Efthymiou, G. and Gazetas, G. (2018), Elastic Stiffnesses of a Rigid Suction Caisson and Its Cylindrical Sidewall Shell, Journal of Geotechnical and Geoenvironmental Engineering 145 (2), 06018014.

Gao, H., Chiu, C.-H. and Lee, J. (1992). Elastic contact versus indentation modeling of multi-layered materials. International Journal of Solids and Structures 29(20), 2471–2492.

Gibson, R. (1967), Some results concerning displacements and stresses in a nonhomogeneous elastic halfspace, Géotechnique 17(1), 58–67.

Gourvenec, S. (2007). Failure envelopes for offshore shallow foundations under general loading. Géotechnique, 57(9), 715-728.

Gourvenec, S., and Randolph, M. (2003). Effect of strength non-homogeneity on the shape of failure envelopes for combined loading of strip and circular foundations on clay. Géotechnique, 53(6), 575-586.

Hardin, B. O. and Black, W. L. (1966), Sand stiffness under various triaxial stresses, Journal of Soil Mechanics and Foundations Division, ASCE: 92(SM2), 667–692.

Hardin, B. O. and Black, W. L. (1968), Vibration modulus of normally consolidated clays, Journal of Soil Mechanics and Foundations Division, ASCE: 94(SM2), 353–369.

Hardin, B. O. and Drnevich, V. P. (1972), 'Shear modulus and damping in soils: design equations and curves', Journal of Soil Mechanics and Foundations Division (ASCE), Vol. 98, No. 7, 667–692.

He, P., and Newson, T. (2020). Undrained capacity of circular foundations under combined horizontal and torsional loads. Géotechnique Letters, 10(2), 186-190.

Houlsby, G. T., Amorosi, A., and Rojas, E. (2005). Elastic moduli of soils dependent on pressure: a hyperelastic formulation. Géotechnique, 55(5), 383-392.

Kassir, M. K. and Chuaprasert, M. F. (1974), A rigid punch in contact with a nonhomogeneous elastic solid, Journal of Applied Mechanics 41(4), 1019–1024.

Kausel, E. (2010). Early history of soil–structure interaction. Soil Dynamics and Earthquake Engineering, 30(9), 822-832.

Kohata, Y., Tatsuokaj, F., Wang, L., Jiang, G. L., Hoque, E., and Kodaka, T. (1997). Modelling the non-linear deformation properties of stiff geomaterials. Géotechnique, 47(3), 563-580.

Lin, G., Han, Z., and Li, J. (2013). An efficient approach for dynamic impedance of surface footing on layered half-space. Soil Dynamics and Earthquake Engineering, 49, 39-51.

Mayne, P. W. and Poulos, H. G. (1999). Approximate displacement influence factors for elastic shallow foundations, Journal of Geotechnical and Geoenvironmental Engineering 125(6), 453–460.

Mayne, P. W. (2019). Settlement of 16-story office tower on raft foundation situated on Piedmont residuum. Proceedings Geo-Congress 2019: Foundations (GSP No. 307), American Society of Civil Engineers, Reston, VA: 412-425.

Niazi, F. S., and Mayne, P. W. (2010). Evaluation of EURIPIDES pile load tests response from CPT data. ISSMGE International Journal of Geoengineering Case Histories, 1(4), 367-386.

Nouri, H., Biscontin, G., and Aubeny, C. P. (2014). Undrained sliding resistance of shallow foundations subject to torsion. Journal of Geotechnical and Geoenvironmental Engineering, 140(8), 04014042.

Poulos, H. G. (1979). Settlement of single piles in non homogeneous soil. Journal of Geotechnical Engineering Division ASCE, 105(5), 627–641.

Poulos, H. G. and Davis, E. H. (1974). Elastic Solutions for Soil and Rock Mechanics, John Wiley and Sons, New York, 411 pages. Download from: www.usucger.org

Reissner, E., and Sagoci, H. F. (1944). Forced torsional oscillations of an elastic half-space. I. Journal of Applied Physics, 15(9), 652-654.

Shen, Z., Bie, S. and Guo, L. (2017). Undrained capacity of a surface circular foundation under fully three-dimensional loading. Computers and Geotechnics 92, 57–67.

Shibuya, S., Hwang, S. and Mitachi, T. (1997). Elastic shear modulus of soft clays from shear wave velocity measurement. Géotechnique 47(3), 593–601.

Selvadurai, A. P. S. (1996), The settlement of a rigid circular foundation resting on a halfspace exhibiting a near surface elastic non-homogeneity, International Journal for Numerical and Analytical Methods in Geomechanics 20, 351–364.

Suryasentana, S. K., Dunne, H. P., Martin, C. M., Burd, H. J., Byrne, B. W., and Shonberg, A. (2020a). Assessment of numerical procedures for determining shallow foundation failure envelopes. Géotechnique, 70(1), 60-70.

Suryasentana, S. K., Burd, H. J., Byrne, B. W., and Shonberg, A. (2020b). A systematic framework for formulating convex failure envelopes in multiple loading dimensions. Géotechnique, 70(4), 343-353.

Vesić, A. (1973). Analysis of ultimate loads of shallow foundations. Journal of the Soil Mechanics and Foundations Division (ASCE) 99, No. 1, 45–73.

Vrettos, C. (1991), Time-harmonic Boussinesq problem for a continuously nonhomogeneous soil, Earthquake Engineering Structural Dynamics 20(10): 961–977.

Vulpe, C., Gourvenec, S. and Power, M. (2014). A generalised failure envelope for undrained capacity of circular shallow foundations under general loading. Géotechnique Letters 4, No. 3, 187–196.

Wroth, C. P., Randolph, M. F., Houlsby, G. T. and Fahey, M. (1979), A review of the engineering properties of soils with particular reference to the shear modulus, Technical report, CUED/D-Soils TR75, Cambridge University Engineering Department, Cambridge, UK.

Yamada, S., Hyodo, M., Orense, R. P., Dinesh, S. V., and Hyodo, T. (2008). Strain-dependent dynamic properties of remolded sand-clay mixtures. J. Geotech. Geoenviron. Eng., 134(7), 972–981.

Table 1. Best-fit Weibull parameters (i.e. a, b) for the parametric weight distributions $\widehat{w}_{\mathrm{param}}$ (Eq. 39) corresponding to the different stiffness.

Stiffness	a	b
Lateral K_H	1.27	$0.237 - 0.049\nu$
Rotational K_M	1.35	$0.17 + 5\nu^4$
Torsional K_Q	1.46	0.076

Table 2. Young's modulus profiles for eight three-layered, non-homogeneous soil profiles analysed in the numerical study. $E_R = 100p_{\mathrm{atm}}$ is the reference Young's modulus of the soil, ν is the soil Poisson's ratio, z is the depth below ground level and D is the diameter of the surface foundation.

		Normalised Young's Modulus, E/E_R		
Name	ν	$z < 0.5D$	$0.5D \leq z < D$	$z \geq D$
P1	0.2	1	2	4
P2	0.2	1	4	2
P3	0.2	2	1	4
P4	0.2	2	4	1
P5	0.49	1	2	4
P6	0.49	1	4	2
P7	0.49	2	1	4
P8	0.49	2	4	1

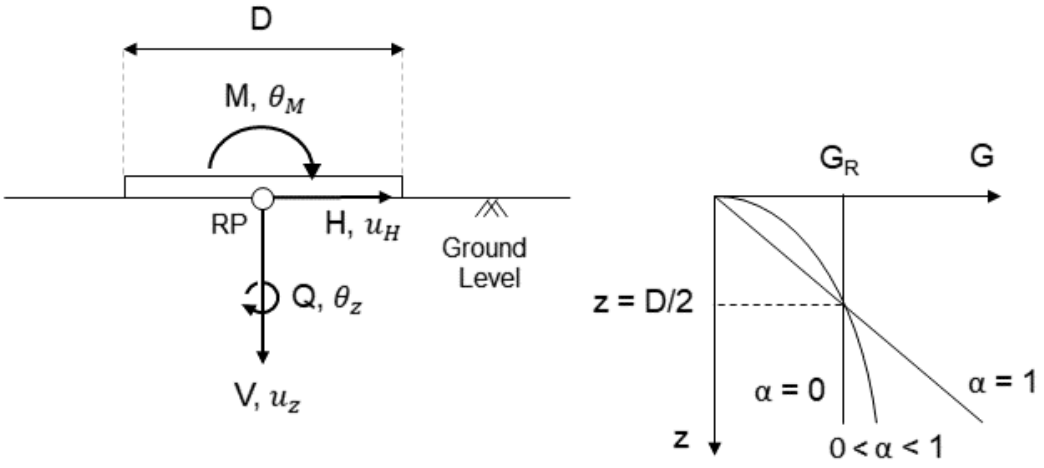

Figure 1 Schematic diagram of a circular surface foundation of diameter $\boldsymbol{D}$ bearing on an elastic half-space with homogeneous and non-homogeneous shear modulus profiles (see Eq. 31).

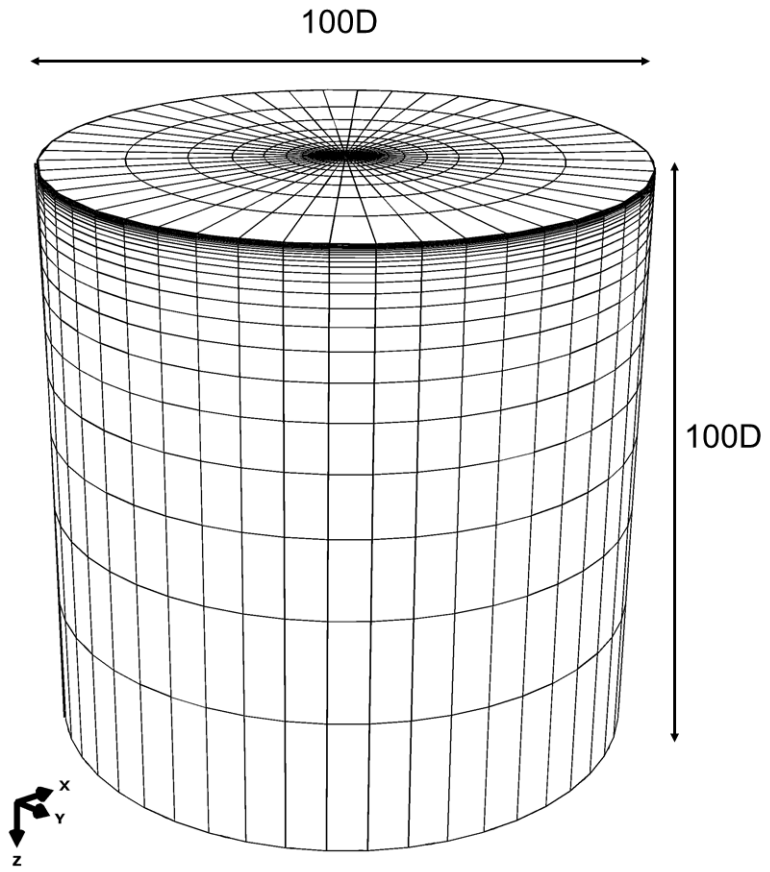

(a)

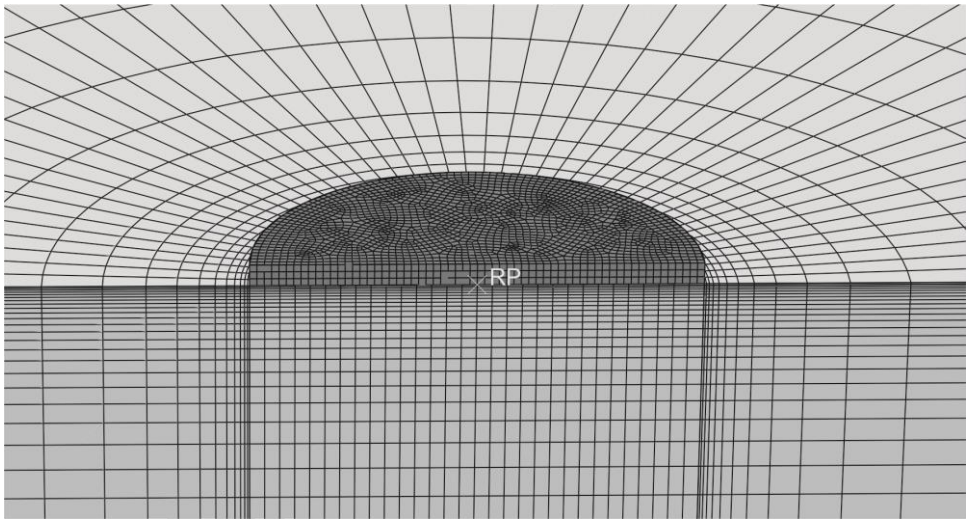

(b)

Figure 2 (a) 3D FEM mesh for a rigid, circular surface foundation on an elastic half-space. (b) Enlarged partial view of the foundation

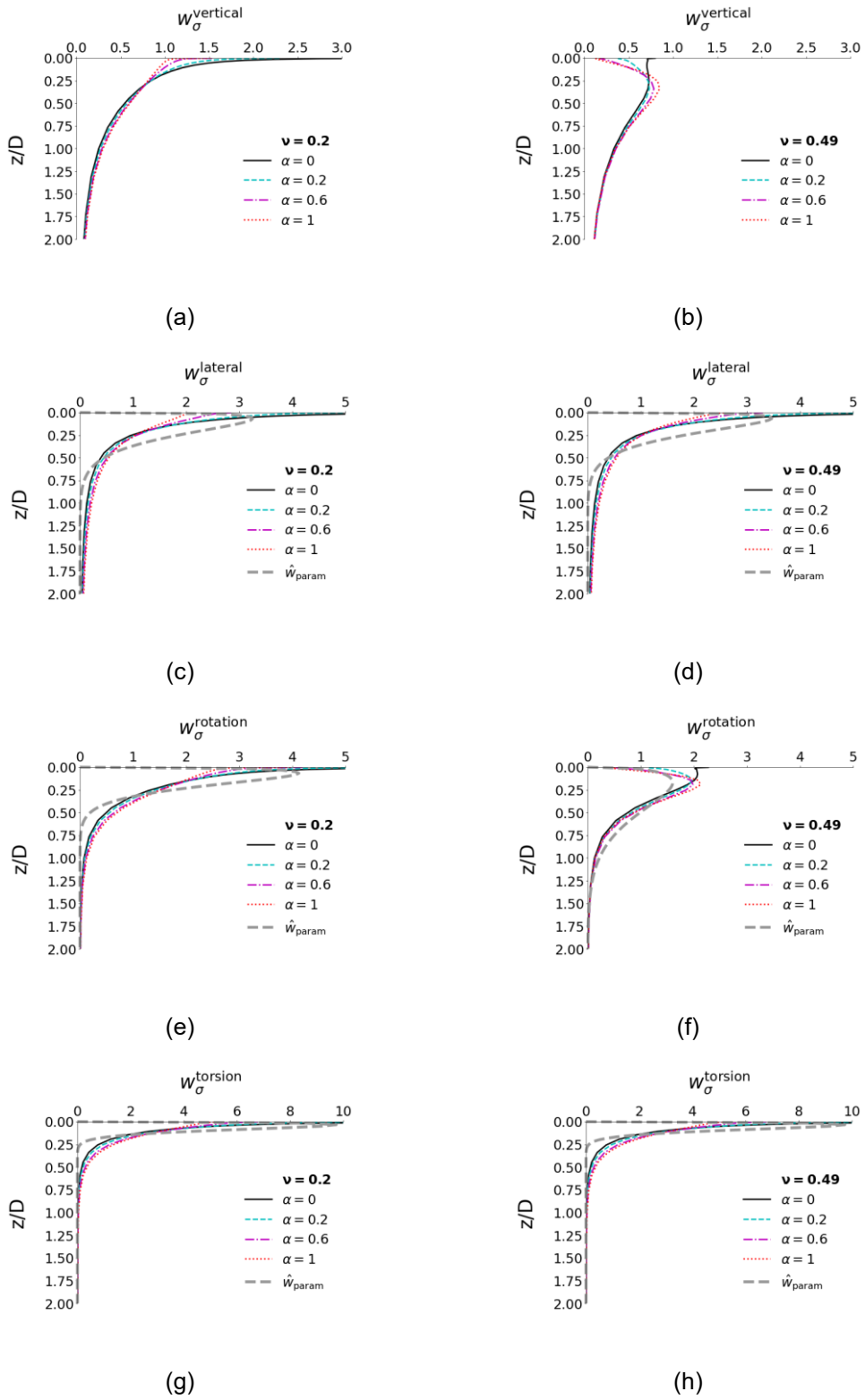

Figure 3 Comparison of w_σ under different prescribed displacements: (a), (b) vertical displacement; (c), (d) lateral displacement; (e), (f) rotation; (g), (h) torsion. Note that $\alpha = 0$ represents the homogeneous elastic half-space case. $\hat{w}_{\mathrm{param}}$ are the parametric weight distributions assumed for the proposed design methods (Eqs. 36 to 38).

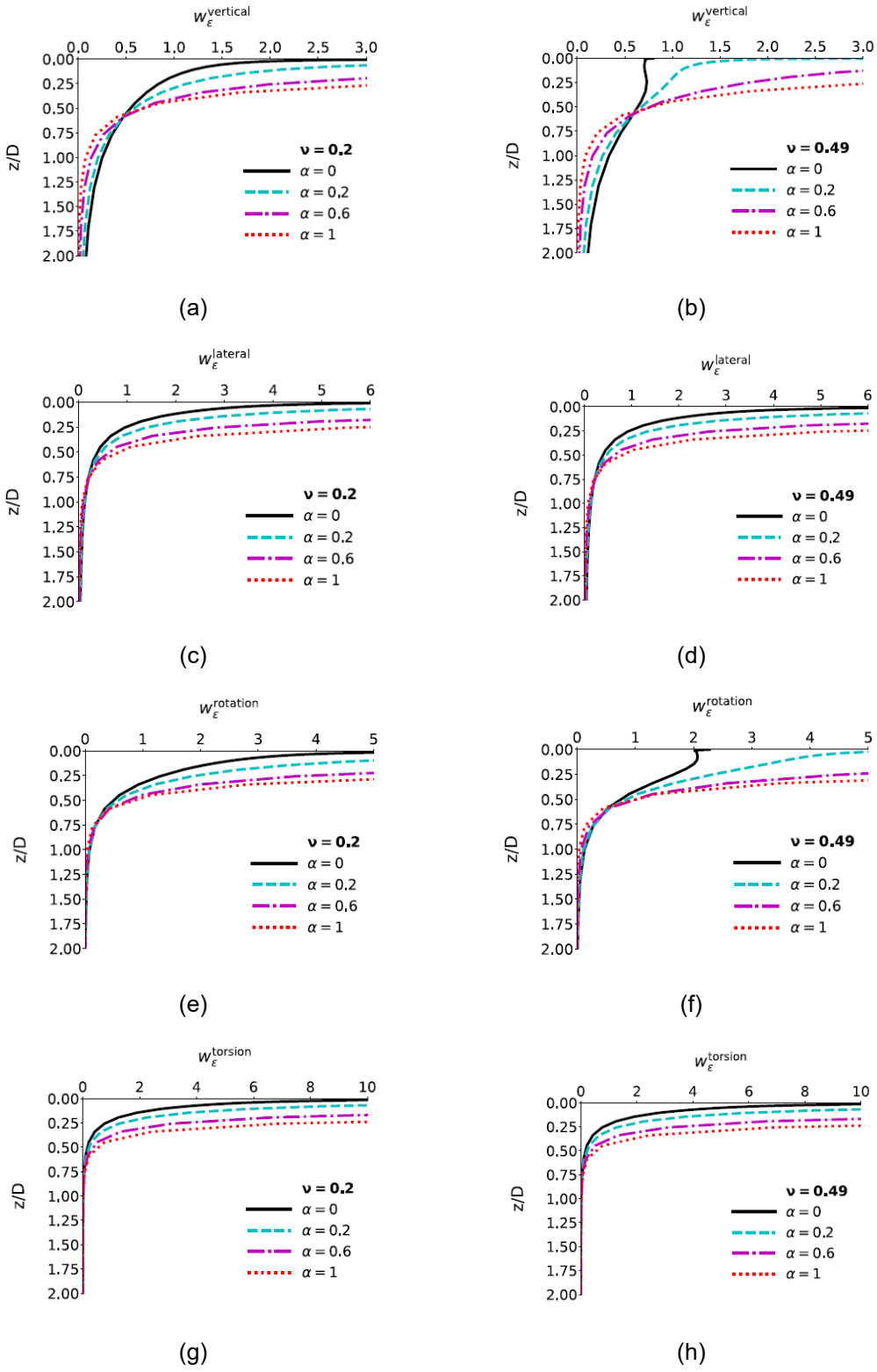

Figure 4 Comparison of w_ε under different prescribed displacements: (a), (b) vertical displacement; (c), (d) lateral displacement; (e), (f) rotation; (g), (h) torsion. Note that $\alpha = 0$ represents the homogeneous elastic half-space case.

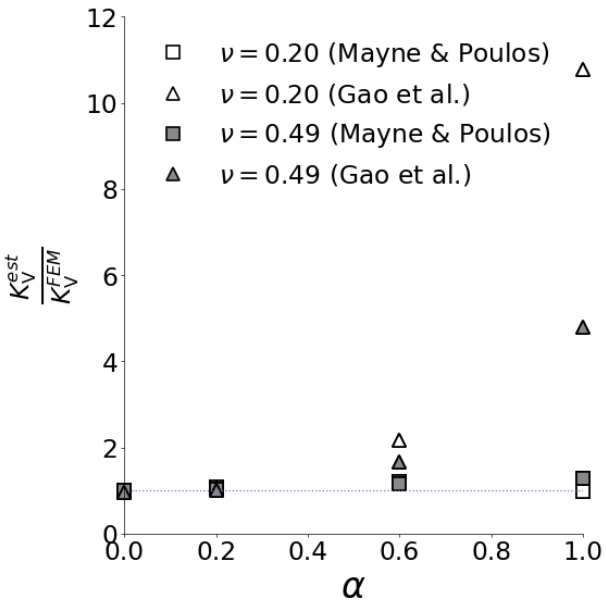

Figure 5 Comparison of the vertical stiffness estimated by the design methods of Mayne and Poulos (1999) and Gao et al. (1992), normalized by the corresponding 3D FEM results, for the continuously varying shear modulus profiles.

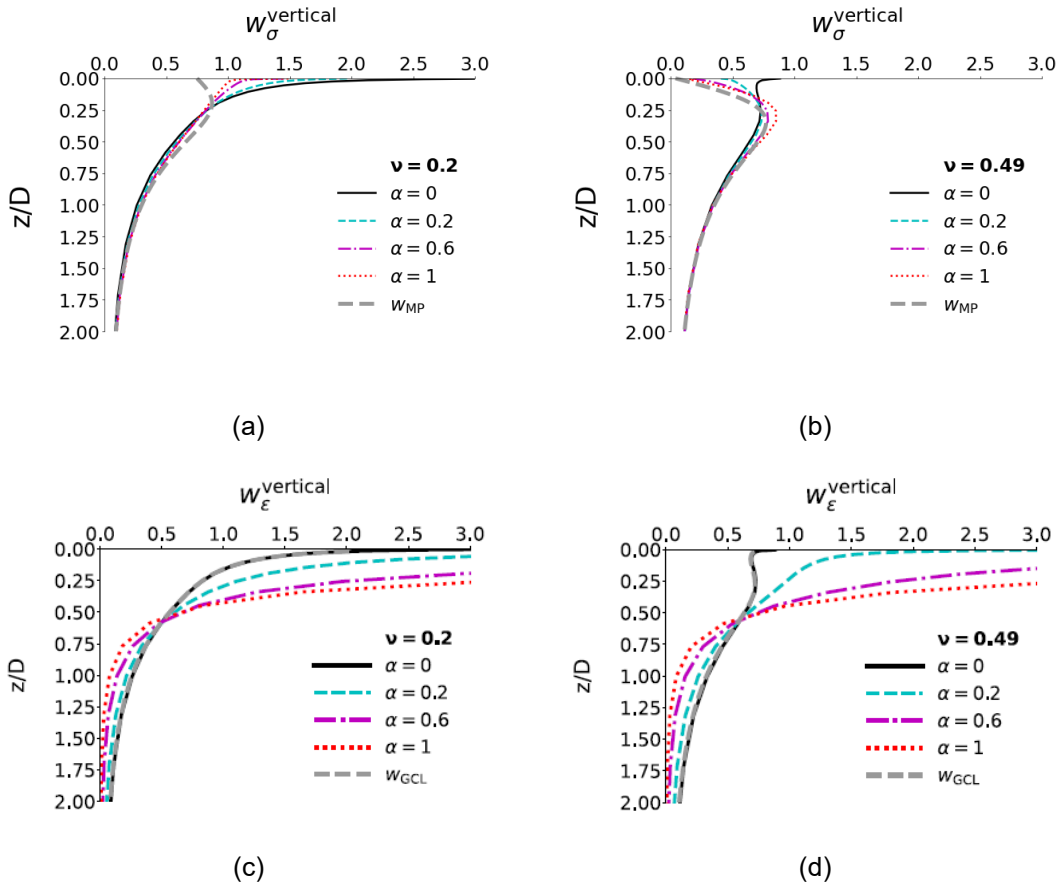

Figure 6 Comparison of weight distributions $\boldsymbol{w_\sigma}$ and $\boldsymbol{w_\varepsilon}$, as calculated from the 3D FEM results for the vertical stiffness problem, assuming smooth contact between soil and foundation. Note that $\boldsymbol{w_{MP}}$ and $\boldsymbol{w_{GCL}}$ correspond to the weight distributions inferred from the Mayne and Poulos (1999) and Gao et al. (1992) design methods, respectively.

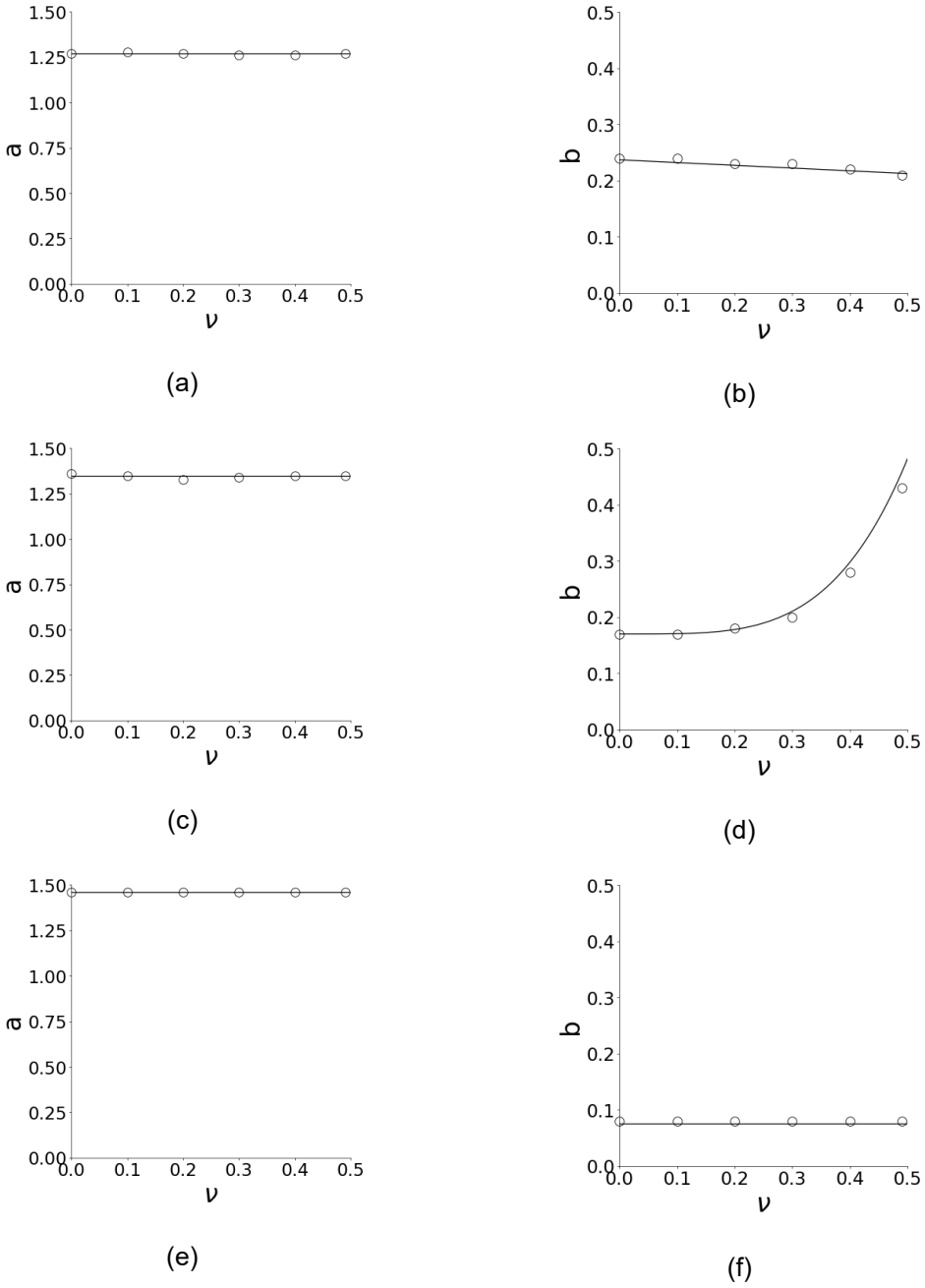

Figure 7 Comparison of the best-fit Weibull parameters ($\boldsymbol{a}, \boldsymbol{b}$) for each Poisson's ratio $\boldsymbol{\nu}$ (shown as white circle markers) and the fitted equations listed in Table 1 (shown as black solid lines) for (a), (b) lateral stiffness; (c), (d) rotational stiffness; (e), (f) torsional stiffness.

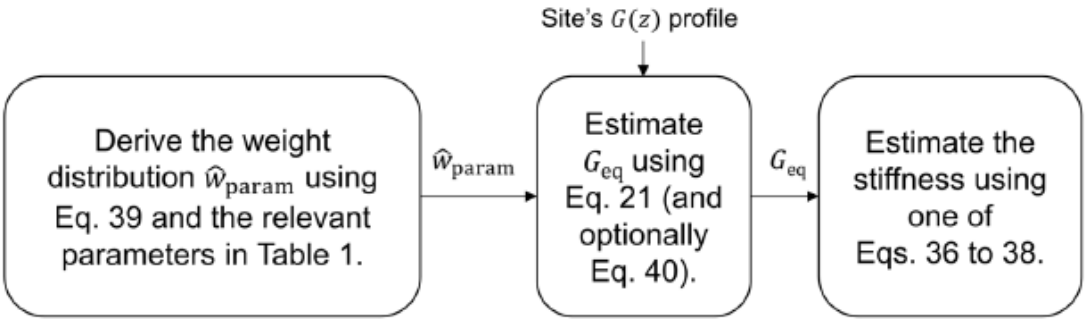

Figure 8 Flow chart showing the steps involved in estimating the stiffness of a foundation on a site with some arbitrary shear modulus $G(z)$ profile.

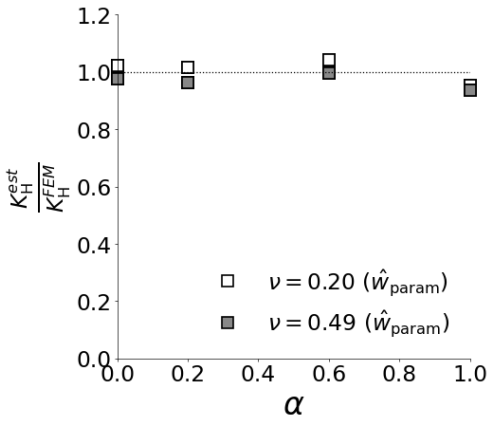

(a)

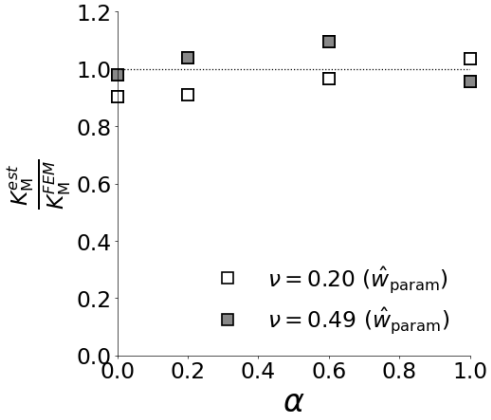

(b)

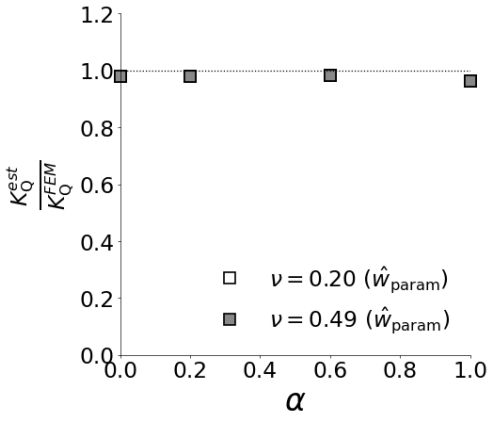

(c)

Figure 9 Comparison of the (a) lateral stiffness; (b) rotational stiffness; (c) torsional stiffness estimated by the new design methods (Eqs. 36 to 38), normalized by the corresponding 3D FEM results, for the continuously varying shear modulus profiles, where $\alpha = 0$ represents the homogeneous elastic half-space case. Note that K_{Q} does not vary with ν.

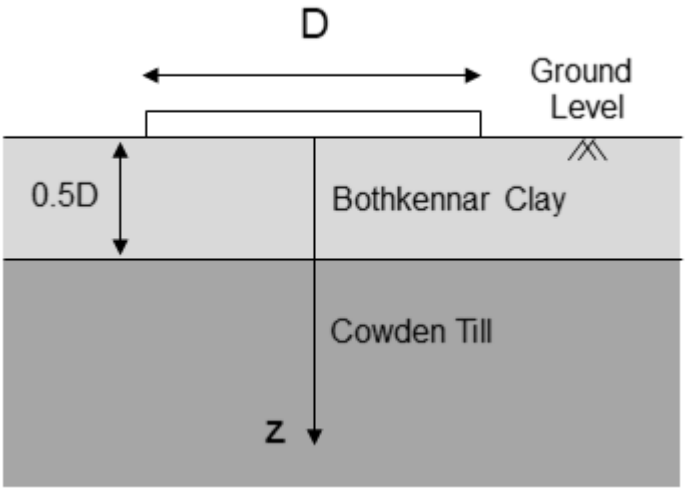

(a)

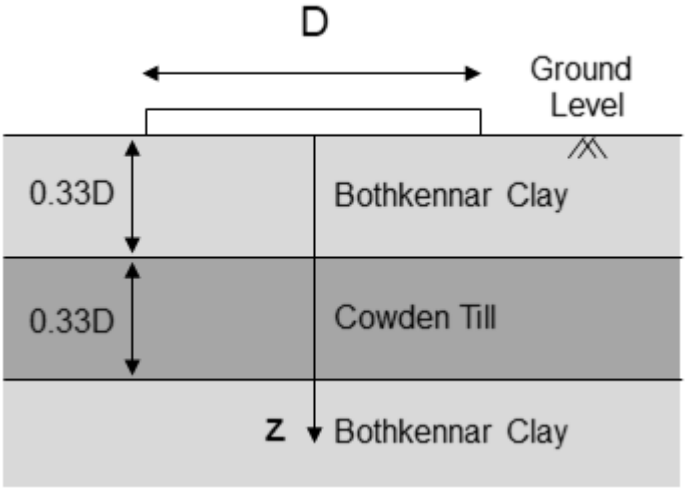

(b)

Figure 10 Schematic diagram of the two multi-layered soil profiles evaluated in this study. Similar soil profiles to these were previously investigated in Burd et al. (2020). (a) 'BC clay' profile comprising of Bothkennar clay overlying Cowden till (b) 'BCB clay' profile comprising of a Bothkennar clay soil matrix with an interbedded Cowden till layer.

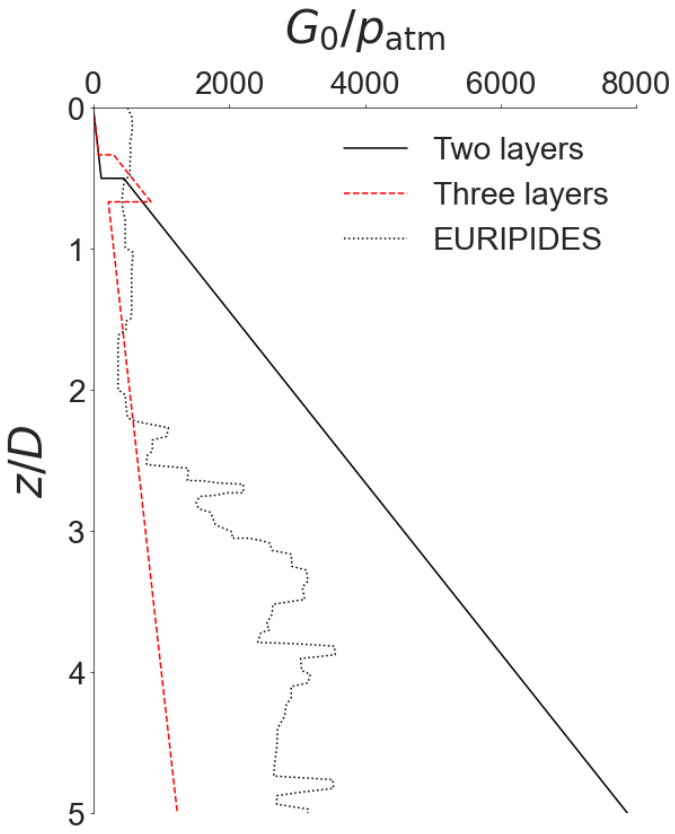

Figure 11 Comparison of the normalized initial shear modulus G_0 of the three complex soil profiles, where the depth is normalized by the foundation diameter D = 10m. 'BC clay' and 'BCB clay' correspond to the soil profiles described in Fig. 10, while 'EURIPIDES' corresponds to the soil profile of the EURIPIDES project (according to Niazi and Mayne 2010).

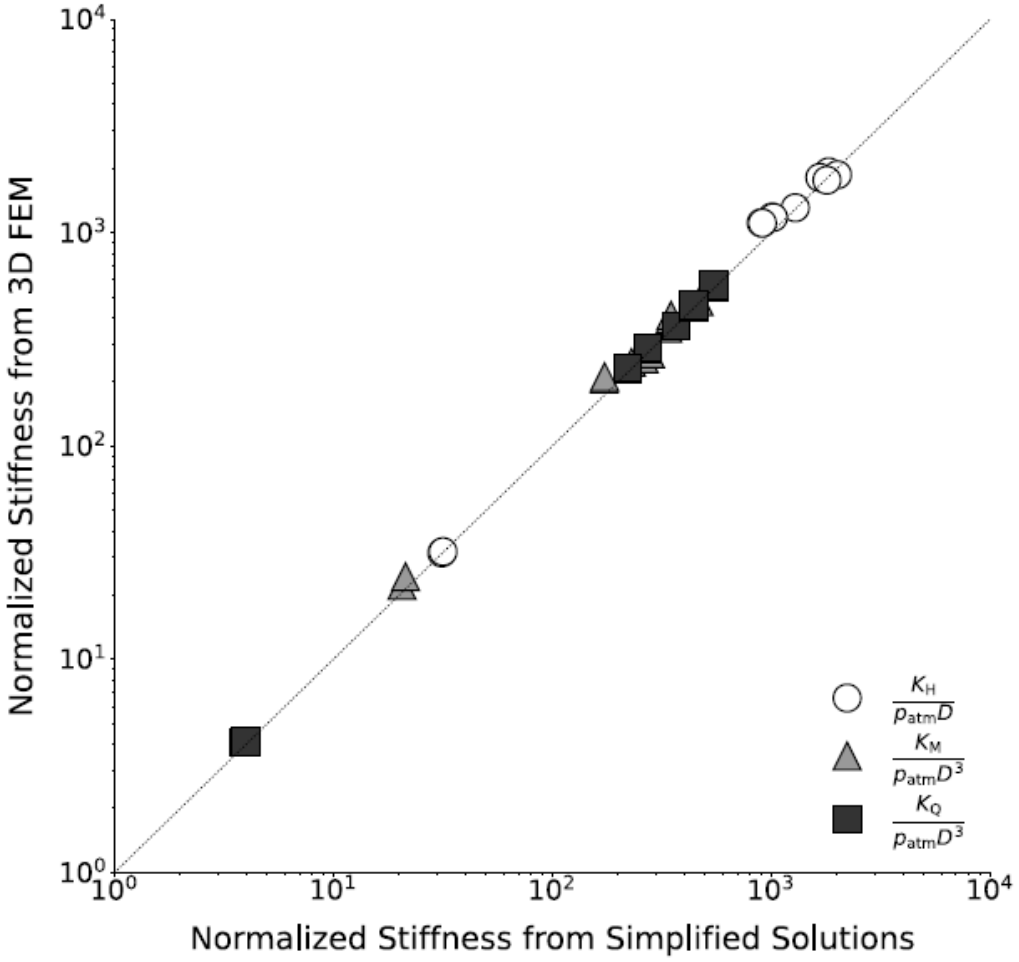

Figure 12 Comparison of the normalized lateral, rotational and torsional stiffness estimated by the simplified solutions (Eqs. 36 to 38) with the corresponding 3D FEM results, for all 11 complex soil profiles. Foundation diameter D is 10m. Both axes are in log scale and the dotted line is a 1:1 line.